Author Manuscript

Author Manuscript

Author Manuscript

Author Manuscript

HHS Public Access

Author manuscript

Cell Rep. Author manuscript; available in PMC 2022 December 11.

Published in final edited form as:

Cell Rep. 2022 October 11; 41(2): 111477. doi:10.1016/j.celrep.2022.111477.

The tempo and mode of gene regulatory programs during bacterial infection

Gal Avital[1,5], **Felicia Kuperwaser**[1,5], **Andrew W. Pountain**[1], **Keenan A. Lacey**[2], **Erin E. Zwack**[2], **Magdalena Podkowik**[3], **Bo Shopsin**[2,3], **Victor J. Torres**[2], **Itai Yanai**[1,4,6,*]

[1]Institute for Computational Medicine, NYU Grossman School of Medicine, New York, NY, USA

[2]Department of Microbiology, NYU Grossman School of Medicine, New York, NY, USA

[3]Department of Medicine, Division of Infectious Diseases, NYU Grossman School of Medicine, New York, NY, USA

[4]Department of Biochemistry and Molecular Pharmacology, NYU Grossman School of Medicine, New York, NY, USA

[5]These authors contributed equally

[6]Lead contact

SUMMARY

Innate immune recognition of bacterial pathogens is a key determinant of the ensuing systemic response, and host or pathogen heterogeneity in this early interaction can impact the course of infection. To gain insight into host response heterogeneity, we investigate macrophage inflammatory dynamics using primary human macrophages infected with Group B *Streptococcus*. Transcriptomic analysis reveals discrete cellular states within responding macrophages, one of which consists of four sub-states, reflecting inflammatory activation. Infection with six additional bacterial species—*Staphylococcus aureus*, *Listeria monocytogenes*, *Enterococcus faecalis*, *Yersinia pseudotuberculosis*, *Shigella flexneri*, and *Salmonella enterica*—recapitulates these states, though at different frequencies. We show that modulating the duration of infection and the presence of a toxin impacts inflammatory trajectory dynamics. We provide evidence for this trajectory in infected macrophages in an *in vivo* model of *Staphylococcus aureus* infection. Our cell-state analysis defines a framework for understanding inflammatory activation dynamics in response to bacterial infection.

This is an open access article under the CC BY-NC-ND license (http://creativecommons.org/licenses/by-nc-nd/4.0/).

*Correspondence: itai.yanai@nyulangone.org.

AUTHOR CONTRIBUTIONS

G.A., F.K., and I.Y. conceived and designed the project, interpreted the results, and drafted the manuscript. G.A. and F.K. conducted most of the experiments. G.A. analyzed the data with contributions from I.Y. K.A.L. and F.K. carried out the *in vivo* experiment. V.J.T. and B.S. contributed to the design of the *S. aureus* experiment. F.K. led the revision. A.W.P. contributed the CellRank analysis and helped with other analysis. F.K., E.E.Z., and M.P. performed the *S. aureus* strain experiment. All authors edited the manuscript.

SUPPLEMENTAL INFORMATION

Supplemental information can be found online at https://doi.org/10.1016/j.celrep.2022.111477.

DECLARATION OF INTERESTS

V.J.T. has consulted for Janssen Research & Development, LLC and has received honoraria from Genentech and Medimmune. V.J.T. is also an inventor on patents and patent applications filed by New York University, which are currently under commercial license to Janssen Biotech Inc. Janssen Biotech Inc. provides research funding and other payments associated with a licensing agreement.

Author Manuscript Author Manuscript Author Manuscript Author Manuscript

Graphical Abstract

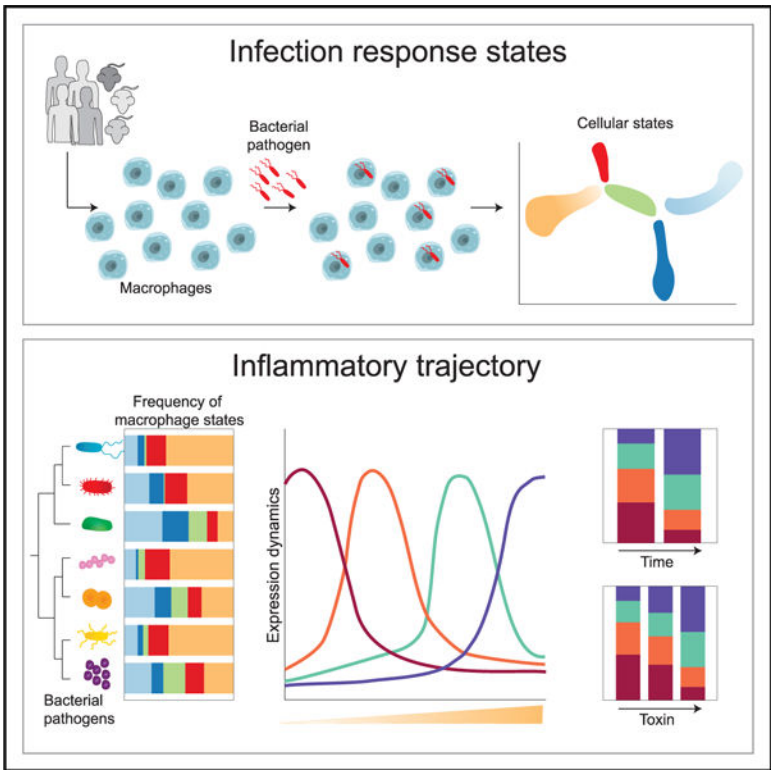

In brief

Avital et al. show that bacterial infection induces discrete transcriptomic states in macrophages that correspond to different response functions. One of these states captures inflammatory activation characterized by four gene modules. The dynamics of this inflammatory trajectory can be impacted by modulation of bacterial stimulus, infection duration, and presence of toxins.

INTRODUCTION

The early interaction between a pathogen and host immune cell is a key determinant of the subsequent immune response with implications for infection outcome. As such, it is critically important to understand different functional macrophage properties at the outset of infection (Akira et al., 2006; Iwasaki and Medzhitov, 2015; Janeway and Medzhitov, 2002; Parihar et al., 2010). Different inputs to this interaction include a host cell's disposition prior to introduction of antigen, as well as the state of the infecting pathogen (Avital et al., 2017; Avraham et al., 2015; Saliba et al., 2016; Shalek et al., 2014; Villani et al., 2017). A host cell's state may be resistant to the pathogen or permissive, allowing intracellular replication or resulting in host cell death (Bumann, 2015; Shin, 2012). Uninfected neighboring cells, bystanders, can detect infection in adjacent cells through cytokine signals, and they, in turn, amplify the host immune response by recruiting additional immune cells to the site of infection (Holmgren et al., 2017).

Author Manuscript Author Manuscript Author Manuscript Author Manuscript

The group of bacterial pathogens that infect human host cells is characterized by diverse attributes. These species all differ within their morphological characteristics, the ability to replicate within a host cell, and host sites of infection. The innate immune system has evolved a conserved response to these phenotypically diverse bacterial pathogens in order to respond quickly to microbial threat while an antigen-specific response develops (Blecher-Gonen et al., 2019; Medzhitov and Janeway, 1997). This response is initiated by macrophage recognition and binding of a pathogen, and pathogen absorption into the phagosome. Subsequent production of reactive oxygen species (ROS), pH modification, and fusion with the lysosome, leads to degradation of the bacteria (Hirayama et al., 2017). Macrophages also present antigen and secrete cytokines and chemokines to initiate, amplify, and specify the ensuing adaptive response (Medzhitov and Janeway, 1997; Murray and Wynn, 2011; Sica et al., 2015). The tissue-level response to a pathogen is orchestrated by the coordinated activity of a population of immune cells, and the response of an individual cell in that setting is likely dictated by the rest of that population. While the components of the macrophage response to pathogenic challenge are well characterized, the relationship between these functions in a population of responding cells and the dynamics of these functions over time following infection has not been described.

Previous work has demonstrated the value of a single-cell approach in addressing host response heterogeneity (Gomes et al., 2019; Peters et al., 2020; Picelli, 2017; Rosenberg et al., 2021; Svensson et al., 2018; Wen et al., 2020). Many of these studies focus on the way that different sources of either bacterial heterogeneity or host cell type or state can impact the fate of an individual macrophage with implications for the course and outcome of an infection. Works analyzing bacterial heterogeneity have shown how virulence factor expression can impact infected host cells, as well as how bacterial growth rate can affect macrophage polarization (Avraham et al., 2015; Saliba et al., 2016). Our group has previously identified different host response states corresponding to different stages of infection based on both host and pathogen factors heterogeneity (Avital et al., 2017).

Here, we investigated cell population-level dynamics within a group of macrophages responding to bacterial infection. A systematic comparison of infected *ex vivo* human macrophages allowed us to define discrete cellular states of infection, including an inflammatory response program, which, in turn, comprises temporally regulated gene module expression. We found that the presence of these response components and their relationship is reproducible across infection by a range of bacterial pathogens, although the population dynamics differ depending on the stimulus. We found that the time of infection or the presence of toxin shifted these dynamics.

Our work defines the set of conserved states expressed by macrophages in response to bacterial infection, whose composition within a population of cells can serve as a measure of innate activation with implications for the course and outcome of infection.

Author Manuscript Author Manuscript Author Manuscript Author Manuscript

RESULTS

An *ex vivo* system for capturing heterogeneity in a macrophage population responding to infection

To capture the host transcriptomic response that accompanies the early stages of bacterial infection in a population of responding cells, we analyzed human monocyte-derived macrophages (hMDM) infected with Group B *Streptococcus* (*Streptococcus Agalactiae*, [GBS]). Macrophages have been implicated in the response to GBS (Flaherty et al., 2019, 2021; Randis et al., 2014), so we used it as a model to interrogate the macrophage response to GBS *ex vivo.* We isolated peripheral blood mononuclear cells (PBMCs) from blood from four healthy human donors, selected adherent monocytes, and differentiated these into hMDM with the growth factor GM-CSF (see STAR Methods). We infected these macrophages with GBS (lab strain, COH1) for 4 h and processed them for scRNA-seq analysis, together with control hMDMs that were not exposed to GBS (Figure 1A). A parallel fluorescent activated cell sorting (FACS) analysis indicated that our experimental design yields ~50% GBS-infected cells (Figures 1B and S1A).

Principal component analysis (PCA) on the scRNA-seq data revealed two groups of cells, captured by PC1, which do not segregate according to GBS exposure or donor (Figures 1C and 1D). PC1-high cells expressed higher levels of MHC class II (*HLA-DRA*, *HLA-DRB1*), iron storage (*FTL*, *FTH1*), and chemokine (*CXCL8*) genes (Figure 1D), and based on this expression pattern, we inferred that the two groups correspond to differentiated macrophages and other cell types captured by the isolation process. The PC1-high cells had high expression of canonical macrophage marker genes (see STAR Methods) (Figure 1D). We selected the differentiated macrophages for further analysis (Figure S1B and see STAR Methods).

PC2 distinguished unexposed from GBS-exposed cells, and infected cells formed a gradient along PC2 (Figures 1C and 1F). Unexposed cells were captured by the low end of PC2, and the high end of PC2 was characterized by high expression of *TNF* and a set of cytokines previously characterized as part of an inflammatory response to bacterial infection, suggesting that PC2 captures the progression of infection (Avital et al., 2017; Avraham et al., 2015) (Figures 1E and 1F; R = 0.73 between PC2 and *TNF* expression). Because we did not synchronize the start of infection in each cell, we have representation of cells from a range of infection stages, given that each cell may have been infected at a different point during exposure to bacteria. To validate that cells along this continuum are indeed infected by GBS, we used flow cytometry to show that cells with intracellular fluorescently labeled GBS also stained positive for TNF (Figures 1G, S1C, and S1D; R = 0.56 between TNF protein expression and GBS-based RFP expression). Hundreds of genes vary in their expression along PC2 revealing a dynamic response of macrophages to infection (Figures 1H and S1E). In particular, we found that genes that are expressed early in infection are exosome-, vesicle-, and granule-related (such as *CD63*, *CD9*, *CTSZ*), and toward the end of this trajectory, we found the expression of inflammatory genes (such as *SOD2*, *TNF*, *IL1B*) (Figures 1H and S1F).

Author Manuscript Author Manuscript Author Manuscript Author Manuscript

Infection-specific macrophage states

We next asked if the heterogeneity captured by PC2 captures a single and continuous response program, or if it reflects the presence of multiple and discrete responses, and we tested this using single-cell trajectory analysis on these macrophages with the Monocle algorithm (Qiu et al., 2017a, 2017b). As Figure 2A shows, analysis of both the GBS-exposed and unexposed cells reveals a branched configuration, composed of five clusters, or states (Figures S2A and S2B and Table S4). Cells that were not exposed to GBS mapped almost exclusively to two of the five states, at one end of the trajectory, while the other three states mostly captured GBS-exposed cells (Figure 2B). tSNE visualization also revealed two large groups in the data, and the unexposed control cells were restricted to one of these groups (Figures S2C and S2D), providing support for the trajectory analysis findings. Based on their uniquely expressed genes, we inferred that the two unexposed states correspond to a non-activated macrophage state and a state with elevated mitochondrial activity (Figure 2C). The former expresses macrophage markers such as *CD68* and *CXCR4*, while the latter expresses genes such as *NDUFC1*, known to be downregulated during bacterial infection to increase ROS by decoupling the respiratory chain (Ramond et al., 2019; Viola et al., 2019).

We wanted to address whether the baseline state of an unexposed macrophage could impact its progress in infection independent of the bacterial stimulation. To do so, we measured the ratio of unexposed macrophages in states 1 and 2 per donor, under the assumption that the same baseline heterogeneity in macrophages from a given donor was present at the start of infection from samples from that same donor. We reasoned that if baseline heterogeneity in each donor captured in unexposed cells would impact a cell's position along the infection trajectory rather than the infection itself, any difference between donors would be mirrored in the degree of activation of cells from the same donor. Instead we found that the pattern of heterogeneity, approximated by the ratio of unexposed cells in state 1 relative to state 2 between donors, was not consistent with the pattern of activation between donors, measured by PC2 scores of infected cells (Figure S2F).

States 3, 4, and 5 all correspond to different functions in cells that were exposed to bacteria (Figure 2B). Cells in state 3 are enriched in genes involved in T cell activation at the immune synapse, including TCR-MHC class II recognition, co-stimulatory molecule (*CD80*), and cytokine secretion (*EBI3*) (Medzhitov and Janeway, 1997). This suggests that cells in state 3 are poised to present antigen through MHC class II to initiate an appropriate adaptive immune response. Cells in state 4 are enriched in genes that are related to pathogen sensing and oxidative stress including *ICAM1*, *IRF8*, *NFKB1*, *TNFAIP3*, *CD40*, and *HIF1A*, suggesting that these cells may be involved in intracellular pathogen killing. State 5 expression is indicative of a cell's role in initiating and amplifying the inflammatory response with high expression of inflammatory genes such as *IL1B*, *CXCL8*, *TNF*, *IL7R*, which are part of characteristic inflammatory response to bacterial infection (Ren and Torres, 2009; Russo et al., 2014; Sedger and McDermott, 2014; Zhou et al., 2015). Mapping states back to the inflammatory trajectory captured by PCA revealed that cells with low PC2 scores were mostly states 1 and 2, and high PC2 scores were mostly state 5, further supporting that PC2 captures an inflammatory activation trajectory (Figure S2E). Given the functional annotations inferred from genes in states 3 and 5, we investigated

Author Manuscript Author Manuscript Author Manuscript Author Manuscript

whether cells in these states are infected by GBS or active bystander cells. To test this, we infected hMDMs with fluorescently labeled GBS, indicating the presence of intracellular bacteria in those cells, and we stained them for representative markers from states 1, 3, and 5 (Figures 2D and S2G). We found that state 5 is composed almost exclusively of GBS-infected cells (Figure 2D). In state 1 and state 3 cells, we found 35% and 24% bystander cells, respectively. We also found evidence for the discrete nature of states 1 and 5 by comparing the staining of markers in individual cells: state 1 and state 5 are largely mutually exclusive in GBS-exposed cells (Figures 2E, 2F, S2H, and S2I). These data suggest that cells with intracellular bacteria are enriched in expression of inflammatory cytokines, while both infected and bystander cells participate in antigen presentation and signaling to the adaptive immune system. We found support for the temporal relationship between some of the observed states using CellRank (Lange et al., 2022), which indicated that states 4 and 5 follow state 1, and that state 3 is an independent and distinct cell state (Figures 2G and 2H).

Gene modules of the inflammatory response and the mid-infection transition

While single-cell trajectory analysis defined state 5 as a discrete cluster, inflammatory gene expression analysis of cells within the cluster suggested a high degree of internal expression heterogeneity. To further resolve the expression patterns within this state, we analyzed the GBS-exposed state 5 cells using PCA. PC1 captured an inflammatory trajectory characterized by an increase in inflammatory gene expression along this axis (Figure S3A). Using K-means clustering, we identified four gene modules that are expressed at distinct stages throughout this trajectory (Figures 3A and 3B; Figure S3A, see STAR Methods). Module 1, expressed first, is enriched for genes with functions characteristic of resting macrophages, including *CD14*, *LYZ*, and *FTH1*. Module 2 is enriched for genes characteristic of activated macrophages that are responding to bacterial infection, including genes such as *FCGR2B* and *C1QC*. Module 3 includes genes with functions for antigen processing and presentation, such as *CD74* and *HLA-DRA*. Finally, module 4 is enriched with genes for T cell activation, such as *IL12B* and *IL18*.

Mapping expression of the module genes to PCA space, we recapitulated the order of expression: the first and last modules are restricted to low and high PC1, respectively, and modules 2 and 3 span the middle of PC1, and the directionality of this trajectory is supported by CellRank (Figures 3C and 3D). Silhouette analysis provided further support for the coherence of the four modules (Figure S3C). The presence of these modules was robust to the number of genes included in the analysis (Figure S3D), and the functional characterization of these modules was robust across databases (Figure S3E). CellRank pseudotime supported our trajectory inference based on PC1 + PC2 scores (Figure S3F). Repeating the analysis using non-negative matrix factorization (NMF) to cluster the genes, we also found that the gene modules are reproducible using both methods of clustering (Figures S3G and S3H and see STAR Methods). We also measured the overlap of the genes in these modules as well as the defined cell states with previously described macrophage gene clusters induced in response to stimulation and found that module 4 has a high overlap with previously described clusters (Figures S3I and S3J) (Cheng et al., 2017, 2019).

Author Manuscript Author Manuscript Author Manuscript Author Manuscript

To analyze the expression dynamics of these four modules, we scored each cell for its relative expression of each module (see STAR Methods). Figure 3E indicates the module scores across the cells, ordered according to their location in the trajectory map (PC1 + PC2). This map recovers the relationship among the modules: 1 and 2 are expressed before 3 and 4, and CellRank pseudotime recovers this order. This visualization also revealed a punctuated, rather than gradual, transition between early and late module expression. Correlating the cells according to their module scores further supported this dynamic pattern of expression, which we refer to as the ‘‘mid-infection transition’’ (Figures 3E and 3F). The punctuated nature of the transition was also evidenced by an increase in the rate of change in the middle of the process compared with the beginning and end (Figure 3G). Collectively, these analyses suggest a discrete transition during infection between two phases in a macrophage inflammatory program: an early phase of sensing and phagocytosis of the bacteria and a late phase of amplification including signaling and T cell response activation.

Conservation of the infection-response gene expression program

The conserved macrophage response to diverse pathogens is well-defined, but we asked if the set of cell states defined in a population of GBS-infected macrophages was pathogen specific. To test this, we repeated our analysis on six additional species: three additional Gram-positive bacteria (*Staphylococcus aureus*, *Listeria monocytogenes*, and *Enterococcus faecalis*) and three Gram-negative bacteria (*Yersinia pseudotuberculosis*, *Shigella flexneri*, and *Salmonella enterica*). These diverse pathogens are distinct in their cell wall composition, mechanism of host cell entry, and their host sites of colonization (Figure 4A). We exposed hMDMs from four human donors to each bacteria species for 4 h of infection and multiplexed samples from each donor for processing with scRNA-seq (Figures S4A and S4B; see STAR Methods). In order to control for variation in the bacterial inoculum and uptake, we grew all bacteria to the stationary phase and infected cells at MOIs that yielded approximately 50% infected cells in each sample at 4 h post infection (Figures 4B and S4A). Despite variation in bacterial growth conditions, we aimed to control for macrophage response rather than focusing on bacteria-specific virulence mechanisms. This strategy allowed us to control the overall response dynamics per sample as well as an individual cell’s response, which will be influenced by the extent of the response of other cells around it.

Once again, we found that the cluster of fully differentiated macrophages explained the most variation in both the exposed and unexposed cells (Figures 4C and S4C). Restricting our analysis to this cluster of differentiated macrophages, we found that PC2 accounted for the trajectory of infection as before (Figure 4C). While we might have expected that the macrophages would have clustered according to the infecting species, we found instead that macrophages infected by different species are well integrated within the PC2 infection trajectory (Figures 4C–4E). Along this axis, cells infected by certain species (*Salmonella*, *Shigella*, GBS, and *Listeria*) were biased toward the later stages of infection (high PC2), while other species (*Yersinia*, *Enterococcus*, and *Staphylococcus*) showed the opposite distribution (low PC2), suggesting different dynamics of infection that do not correspond to the distinguishing attributes between these species (Figure 4E).

Author Manuscript Author Manuscript Author Manuscript Author Manuscript

Monocle analysis on the cells infected by all seven species revealed a similar pattern in the data to that of the GBS-specific analysis (Figure 4F): two states of non-activated macrophages (states 1 and 2, to which the unexposed cells are restricted), an antigen-presentation state (state 3), a pathogen response state (state 4), and a highly inflammatory response state (state 5) (Figures 4F, S4D, and S4E). Thus, despite the range of attributes in these infecting species, the observed macrophage states in response to bacterial infection are robust and conserved. The relative frequencies of the states across the bacterial infections, however, do vary (Figure 4G).

We next asked whether the inflammatory modules defined in cells with intracellular bacteria are also conserved among the different bacteria. We used K-means clustering on the state 5 cells infected by any one of the seven pathogens, and we found four gene modules with similar profiles to those found in the GBS-specific analysis (Figures 4H and S4F and Table S5). To measure the similarity between the GBS-specific modules and these, we measured the significance of the overlap between the two sets using the hypergeometric distribution and found a high enrichment (p value $< 10^{-50}$, Figure S4G). We computed the mean expression of each gene module for each cell and assigned that cell to the module with the highest expression (see STAR Methods) in order to measure the expression of these modules in response to the different bacteria. We found that all modules are represented in state 5 infected macrophages across the bacteria (Figure 4I). The ‘‘resting macrophage’’ module shows the highest frequency among the state 5 cells, suggesting that bacterial detection is the state with the longest duration during the infection process. Since the gene modules are detected across the range of infections, we conclude that they constitute part of the conserved infection response.

Dynamics of infection states

Our data suggest that the composition of states underlying the conserved macrophage response is reproducible, but shifted, in response to different stimuli. We therefore asked if we can manipulate population structure by modulating clinically relevant factors like infection duration and the presence of toxin. To test whether infection duration impacts the composition of population states, we repeated the *ex vivo* experiment comparing two time points of infection by exposing hMDMs differentiated from three donors to all seven species and collecting samples at 2 and 4 h after exposure (Figure 5A). We found that the differentiated macrophages from the 2 and 4 h of infection distributed differently along PC2 (Figures 5B and S5A): cells stimulated for 4 h are shifted to higher PC2 scores relative to the cells stimulated for 2 h, indicating a more advanced inflammatory response after 4 h of infection.

We analyzed the dynamics of the states by comparing their frequencies between the times of infection for each species of infection. For this, we mapped cells from both time points to our five Monocle-defined states and confirmed the observed temporal shift with CellRank pseudotime (Figures 5C and S5B–S5E and STAR Methods). We found that all five states are also present in the 2 h time point. Moreover, for all seven infecting species, we found greater representation of state 5 from the cells stimulated for 4 h ($p < 0.02$, paired t test). Consistent with the previous results (Figure 4), infection by different species is distinguished by unique

Author Manuscript Author Manuscript Author Manuscript Author Manuscript

patterns of states' frequencies, providing further evidence that while the overall processes are conserved, the dynamics for individual bacterial species differ. The only consistent shift between time points and across conditions was the greater representation of state 5 cells at 4 h post infection, suggesting that the state 5 activation trajectory reflects time or extent of infection. Comparing the frequencies of gene modules across the two timepoints (see STAR Methods), we found that modules 1 and 2 were present at higher levels in the 2 h time point cells than modules 3 and 4 (Figure 5D), supporting our inference that gene modules are induced serially as infection progresses.

Having established the temporal dependence of the state 5 inflammatory activation trajectory, we asked whether bacterial factors could modulate the extent of population-level activation, and therefore if it reflects a feature of clinically relevant infection. In our multi-species comparison, we normalized all strains to conditions that would stimulate macrophages to the same extent in order to compare host population dynamics while limiting bacterial variability. In order to test for the effect of bacterial virulence factors on the host response, we instead compared the response to infection with clinically isolated *Staphylococcus* strains, comparing infection between a wild-type *S. aureus* strain (WT USA300, Lac) and an isogenic strain missing multiple phagocyte lytic toxins (Δtox USA300; Δ*lukAB, hlg::tet, lukED::kan, pvl::spec, hla::erm*), ''toxin-less'' (Bhattacharya et al., 2018) at a higher MOI in order to increase toxin impact. We selected CD14+ cells from PBMCs, which produced a purer population of macrophages, and as before, differentiated them into hMDM with GM-CSF (see STAR Methods). We infected day 4 macrophages with the toxin-less and WT strains along with uninfected controls for 4 h (Figure 5E). Because of the macrophage selection method used, PC1 does not capture a mix of macrophages and other cells, but rather an infection trajectory, illustrated by high expression of TNF (Figure 5F). Comparing PC1 scores between conditions reveals that infection with the toxin-less strain yielded significantly lower ($p < 10^{-3}$) scores than with WT *Staphylococcus* (Figure 5G). Cells equivalent to state 5 were selected based on their expression of TNF (Figure S5F) and the ratio of modules between them was measured revealing greater representation of later modules in the WT compared with the ''toxin-less'' USA300 strain (Figure 5H). We also infected cells with seven other strains (Table S2; Lacey et al., 2022; Rose et al., 2015) to control for the effect of these toxins rather than other strain-specific differences and found no significant difference in trajectory analysis, suggesting that this shift in trajectory was indeed toxin-mediated (Table S2 and Figures S5G–S5I).

In vivo analysis of macrophage inflammatory programs

Having established that the state 5 inflammatory activation trajectory reflects the extent of infection, we wanted to see if there was any evidence for the presence of this trajectory in a complex infection setting. We thus tested for the presence of the infection modules and relationship between them in an *in vivo* setting. For this we analyzed macrophages from a mouse model of *S. aureus* infection. Mice were injected intraperitoneally with bacteria or PBS control, and after 1 h, cells were collected by peritoneal lavage. Infected macrophages were identified by expression of fluorescently labeled intracellular bacteria and were sorted by flow cytometry for scRNA-seq analysis (Figures 6A and S6A; see STAR Methods).

Author Manuscript Author Manuscript Author Manuscript Author Manuscript

On the basis of marker gene expression, macrophages were identified for further analysis (Figure S6B).

PCA of the infected macrophages reveals a trajectory characterized by heterogeneous expression of inflammatory markers between cells (Figure 6B). We defined an inflammatory trajectory that ordered the cells by the sum of their PC1 and PC2 scores based on the pattern of *Il6* expression (Figure 6C). In order to test for the presence of our previously defined infection modules in this *in vivo* setting, we examined expression of selected module genes and Gene Ontology (GO) terms across the trajectory, which broadly matched the expression pattern in the *ex vivo* system (Figure 6D). Cells from the PBS-infected control samples were analyzed in parallel and showed no dynamic expression of these genes (Figure S6C). We also computed expression levels of the mouse orthologs corresponding to the human modules, which recapitulated the expression pattern of these modules in our mouse data (Figure 6E). Correlation analysis between infected macrophages along the inflammatory trajectory also recapitulated the mid-infection transition observed between the two inflammatory program phases in the human *ex vivo* infected macrophages (Figure 6F). These data provide a robust *in vivo* support for the human *ex vivo* results.

DISCUSSION

In this work we have analyzed the macrophage response to diverse bacterial pathogens. We found that a population of responding macrophages includes cells in different transcriptomic states that together constitute the full spectrum of gene expression during this process. Our results led us to define a model for the mode and tempo of macrophage state expression during infection, shown in Figure 6G. Upon encountering bacteria, a subpopulation of cells remains inactive, resembling unexposed cells (states 1–2), while others are activated and respond to the invading pathogen (state 3–5). Cells in state 4 express genes related to oxidative killing of intracellular bacteria. Most of the activated cells are highly inflammatory (state 5), expressing *TNF*, *IL1B* and *SOD2*. Some cells, including the activated bystander cells, are poised to present antigen (state 3), expressing MHC-II complex genes for TCR recognition, co-stimulatory genes, and cytokine genes. We expect that state 3 cells are upregulating expression of antigen presentation-related genes in response either to inflammatory cytokine secretion by neighboring infected cells in state 5 or in response to bacteria or bacterial components sensed directly by these cells. The fact that there is more complexity to the composition of states within a population of cells raises the possibility that some cells are inherently resistant to activation or limit their activation in response to inflammatory cells as a means of inflammatory regulation.

Considerable efforts have been devoted to classification of innate immune responses during infection in order to understand how the initial response to pathogen impacts the downstream adaptive response and ultimately outcome. Works focusing on the impact of pathogenic attributes on infection response include analysis of the response to Gram-positive versus Gram-negative bacteria (Björk et al., 1992; Feezor et al., 2003) as well as stimulus-specific responses (Blecher-Gonen et al., 2019; Cheng et al., 2019; Nau et al., 2002; Sheu et al., 2019). Numerous studies focus on heterogeneity of host cell responses with implications for infection outcome in the host including one work predicting outcome based on cell-type-

Author Manuscript Author Manuscript Author Manuscript Author Manuscript

specific signatures in PBMCs (Bossel Ben-Moshe et al., 2019) as well as analysis of the temporal patterns and regulatory control of the macrophage response to pathogenic stimuli (Cheng et al., 2017; Hao and Baltimore, 2009; Tong et al., 2016) (Figures S3I and S3J). The dataset we present here of macrophage gene expression throughout bacterial infection will add to the growing body of work that aims to define in precise terms the specific strategies that confer successful immunity. Further classification of cell-type-specific responses and the integration of these cell-type-specific responses with *in vivo* infection models will help refine our collective understanding of this complex multi-component process.

We build on the stratification of the components of the innate response by addressing the composition of states within a population of responding cells. We found that the same states that reflect elements of the well-characterized conserved innate response to bacterial pathogens were present across different infection conditions. Some of these states together constitute an activation trajectory, which can be modulated depending on the presence of toxin and time of infection. The analytic framework we present demonstrates not just the way a cell's response to infection may change over time, but how responses are expressed in parallel in a population of cells, with important implications for the extent and course of the ensuing host response in different infection settings.

Limitations of the study

Our study contains several limitations that are important to consider in interpreting our results. First, our conclusions are based on the heterogeneous transcriptomic responses captured in a population of macrophages. We recognize that the variation we observed at the transcriptomic level can stem from a number of sources in addition to bacterial stimulation. Variation in cell type, the extent of macrophage differentiation, or the time of bacterial uptake could impact the extent to which a cell can be activated following bacterial recognition. We conclude that these confounding factors do not account for the main source of variation in a population of responding cells, but it will be important to address exactly how the baseline state of a macrophage dictates the extent to which it can be activated.

While this study focuses on the host response to bacteria, it is of course important to consider whether the presence of bacteria and even its activity intracellularly impacts the host cell's response. Our study design did not include labeling for the presence of intracellularly bacteria in the *ex vivo* data. While we attempted to address this in Figure 2D by showing the relative shift in bystanders between states 3 and 5, and the difference in PC2 scores between states (Figure S2E), the baseline state that prevents a cell from taking up bacteria, as well as the role of by-standers in the progression of inflammation is a very important question that requires further study. Finally, work into the mechanism underlying the relationship between these states and modules, through perturbation studies that impact module composition or trajectory activation, would shed more light on the role and significance of the response framework we define with important implications for the systemic response to infection.

Author Manuscript Author Manuscript Author Manuscript Author Manuscript

STAR★METHODS

RESOURCE AVAILABILITY

Lead contact—Further information and requests for resources and reagents should be directed to and will be fulfilled by the lead contact, Itai Yanai (itai.yanai@nyulangone.org).

Materials availability—This study did not generate new, unique reagents.

Data and code availability

- Single-cell RNA-seq data have been deposited at GEO (GSE145862) and are publicly available as of the date of publication. Accession numbers are listed in the key resources table.
- All original code has been deposited at GitHub and Zenodo (https://doi.org/10.5281/zenodo.7011311) and is publicly available as of the date of publication. DOIs are listed in the key resources table.
- Any additional information required to reanalyze the data reported in this paper is available from the lead contact upon request.

EXPERIMENTAL MODEL AND SUBJECT DETAILS

hMDM preparation from human blood by density gradient—Blood from human donors was recovered from leukopacks (NYC Blood bank) and diluted with PBS to up to 50mL. Multiple human donors were used as biological replicates. Ficoll density gradient centrifugation was used to isolate the PBMCs layer. PBMCs were washed with complete media (RPMI, 10% FBS, 10 mM HEPES), and red blood cells (RBCs) were removed with an ACK lysis buffer. Cells were washed with complete media, and plated on tissue culture-treated plates. To select for monocytes, the non-adherent cells were washed off the plate after 1.5h. PenStrep (1:100) and GM-CSF 50 ng/mL were added to the plate, and the cells were incubated at 37°C with 5% CO_2 for 4 days. On Day 2, GM-CSF was added again to the plates.

hMDM preparation from human blood by CD14+ selection—Primary human peripheral blood mononuclear cells (PBMCs) from anonymous, healthy donors (New York Blood Center) were isolated by Ficoll gradient separation as previously described (Reyes-Robles et al., 2016) $CD14^+$ monocytes were then isolated from the PBMC fraction by positive selection using the EasySep™ Human CD14 Positive Selection Kit II (STEMCELL Technologies) according to the manufacturer's protocol. Cells were plated at 1×10^6/mL in RPMI supplemented with 10% FBS, 10 mM HEPES, 100 U/mL penicillin, 100 μg/mL streptomycin and 50 ng/mL GM-CSF. The cells were incubated at 37°C with 5% CO_2. Media was replenished with GM-CSF on day 2. Cells were harvested and plated for infection on day 4.

Bacterial strains—Fluorescently-labeled bacteria were cultured overnight (16h) as indicated in the table below (Table S1). Bacteria were spun down for 10 min at 4000 RPM, resuspended in infection media (RPMI, 0.05% HSA - 10 mM HEPES) and OD600

Author Manuscript Author Manuscript Author Manuscript Author Manuscript

was measured. OD was adjusted for each bacteria according to the MOI indicated in the Table S1. Bacteria were incubated for 30 min with 20% human serum or infection media for Gram-positive and Gram-negative bacteria, respectively. Bacteria were washed twice with infection media and passed through an insulin syringe to prevent clumping. The bacteria were diluted to the MOI indicated in the table below (Table S1). Clinical isolate Staphylococcus strains used in Figures 5 and S5 were grown overnight at 180 RPM and diluted to MOI 5 for infection.

***Ex-vivo* hMDM infection—**Day 4 macrophages were lifted from their plate by vigorously washing the cells off the plate with the media. Cold PBS with EDTA (10 mM) was added to the wells, and the plates were incubated at 4C for 10min, followed by a second vigorous wash, and resuspended in infection media (RPMI, 0.05% HSA - 10 mM HEPES). Cells were manually counted with trypan blue, resuspended to 1–2X10^6 cells/ml, and plated in 12-well plates. hMDMs were infected at the indicated MOI per bacteria so that approximately 50% of the cells would be infected after 4 h of infection, or infection media as control (Figures S4A). For *Enterococcus*, stimulating cells with the MOI that would yield 50% infected cells resulted in significant cell death, so we reduced the MOI for that condition. The Staphylococcus strains used in Figures 5 and S5 were infected at MOI 5 for 4 h. Infected cells were spun down for 5 min at 1200 RPM for infection synchronization, and incubated at 37°C with 5% CO_2 for 2 or 4 h.

Peritoneal infection of mice with USA300 strain—C57BL/6 mice were purchased from Jackson Laboratory and bred onsite to generate animals for experimentation. Age and gender-matched 8–10 week old mice were used. The USA300 MRSA strain was grown overnight in TS broth (37°C, 180 RPM). Bacteria was then subcultured in TSB for 3h at 37°, 180 RPM. Bacteria was washed with PBS and adjusted to 1×10^7 CFU/mL. Three mice were injected intraperitoneally with 300μL. After 1h, cells were collected by peritoneal lavage. Red blood cells were lysed with BD Pharm Lyse Lysis Buffer and cells were stained with antibodies to identify macrophages. Infected macrophages were sorted (SY3200 cell sorter, HAPS1 (100um)) and samples were pooled from the three mice for scRNA-Seq analysis (Figure S6A). Cells were captured using the 10X Chromium platform and processed according to manufacturer recommendations. All animal studies were performed as per an NYU Grossman School of Medicine Institutional Animal Care and Use Committee (IACUC) approved protocol to the Torres Lab.

METHOD DETAILS

Single cell and library preparation for scRNA-Seq—hMDMs were lifted from the 12-well plate by vigorously washing the cells off the plate with the media. Cold PBS with EDTA (10 mM) was added, and plates were incubated at 4C for 10min, followed by a second vigorous wash, and a PBS wash. The different infection conditions were tagged based on expression of cell surface markers B2M and CD298 using the Cell Hashing method (Stoeckius et al., 2018) following their protocol (Table S2). Eight samples (7 bacteria and an unexposed control) or ten samples (9 *Staphylococcus* strains and unexposed) from the same donor were pooled into a single cell suspension in equal amounts (Figure S4B), and ran on the 10X Genomics Chromium Controller with Single Cell 3′ v3 system. The remaining cells

Author Manuscript Author Manuscript Author Manuscript Author Manuscript

were analyzed on a FACS- SONY SH800 to quantify the proportion of infected cells using the fluorescent label of the bacteria inside the cells (Figure S4A). cDNA amplification and library preparation of the mRNA was processed according to 10X Genomics Single Cell 3′ v3 manufacturer's instructions. For the hashtag oligos, 1ul of HTO PCR additive primer was added to the 10X cDNA amplification step, and the supernatant from the 0.6X cDNA cleanup was kept and processed according to the Cell Hashing protocol, with 14 PCR cycles and a 1.2X cleanup after the PCR.

Sequencing—Paired-end sequencing was performed on a Next-Seq or Nova-Seq (Table S3), with read format as indicated in the table. Hashtag libraries were sequenced on the same flow-cells at 1/10 proportion of the mRNA.

Validating infection trajectory and states using FACS—hMDMs were prepared as indicated above and infected with GBS or unexposed to bacteria as a control. The hMDMs cell suspension was stained with Pe/Cy7 TNF anti-human antibody (BioLegend 502,929) or with antibodies for representative genes for the states: state 1- Brilliant Violet CXCR4 anti-human (BioLegend 306,517), state 3- Pe/Cy7 CD80 (BioLegend 305,217) and for state 5- APC IL7R anti-human (BioLegend 351,315) according to the BioLegend intracellular staining protocol. The bacterial fluorescence together with the marker staining was recorded on a FACS- SONY SH800 sorter and analyzed using FlowJo software v10.6.1. PE positive cells were considered infected with GBS. This experiment was done 3 times. Figures 2D–2F shows a representative experiment.

QUANTIFICATION AND STATISTICAL ANALYSIS

hMDMs single cell processing and filtering—Cell Ranger pipeline (V.3.0.0) was used for demultiplexing, mapping to the human genome (GRCh38) and counting umis for individual cells. CITE-seq-Count pipeline was used for demultiplexing and counting the hashtag barcodes. The Seurat package multi-modal data was used to assign each hashtag barcode to a cell barcode, and only cells that had a single hashtag were further processed. Cells were filtered out if they had less than 1000 unique molecular identifiers (UMIs), and if more than 30% or 15% of their transcripts were ribosomal or mitochondrial genes, respectively. Expression was normalized to transcripts per median (TPM) and transformed using Freeman-Tukey transform (FTT). For the Figure 5 Staphylococcus data, filtering thresholds were 700 UMIs, 20% ribosomal genes and 15% mitochondrial genes and analysis was performed on TPM-normalized, log-transformed data.

hMDM single cell data analysis—PCA on transformed (FTT) filtered cells was calculated using informative genes which were defined as highly expressed and variable genes (fano-factor and mean expression above mean-dependent thresholds). The thresholds for each analysis are noted in the figure captions. To select for the fully differentiated macrophage cluster, hierarchical clustering on transformed filtered cells was computed using the same informative genes. We calculated for each cluster the mean expression level and filtered out the cluster with the lower total number of UMIs (non-differentiated macrophages).

Author Manuscript Author Manuscript Author Manuscript Author Manuscript

Macrophage score—For each cell, the sum expression of macrophage-specific genes was calculated using: *HLA-DRA*, *HLA-DRB1*, *HLA-DR, CD4*, *APOE*, *CD68*, *CD64*, *CD86*.

States assignment using monocle—Monocle (Qiu et al., 2017a, 2017b) was used to order the single-cells along a trajectory and define clusters using their informative genes. It assigned cells to these clusters, which we annotated as infection states. For each state we identified differentially expressed genes by performing the Wilcoxon rank-sum test for each state comparing the genes expression level (TPM) between each state and all other states, and selected the top 100 genes with p-value lower than 0.005. For each gene set we calculated the enrichment for Gene Ontology (GO) terms using the hypergeometric test to characterize the state. GO enrichment characterization of states was robust to a p-value threshold of 0.0001 and selection of 75 genes per state. States that had few cells (fewer than 20) and therefore few differentially expressed genes compared to the other states were merged with a neighboring state along the trajectory close state on the trajectory.

Inferring single cell states—States of single cells collected from 2 to 4 h infection timepoints (Figure 5), were inferred based on their gene expression similarity to the single-cells in the original trajectory. Using a KNN classifier (k = 1) we have predicted for each cell in the new dataset, its state based on the expression profiles of its nearest neighbor in the original dataset- Figures 2A and 3E, respectively.

Trajectory analysis with CellRank—To confirm the temporal progression of observed single cell states, we applied CellRank v1.5.1 (Lange et al., 2022). Expression was size-normalized and log-transformed, then 30 principal components and moments were calculated for the informative genes defined above. Next, cell trajectories were computed using the CytoTRACE kernel (Gulati et al., 2020; Lange et al., 2022) and the transition matrix was computed with *threshold_scheme* set to ‘‘soft’’ and *nu* of 0.5. Projections shown are based on PCA as determined within CellRank.

Gene modules clustering using *k-means*—PCA was performed on macrophages annotated as state 5, using 421 informative genes specific to state 5 selected with mean threshold = 3 and fano threshold = 2. Individual cells were binned to ten bins according to their location along PC1, with at least ten cells per bin. A binned expression profile was calculated based on the average expression of each gene per bin. We used *k-means* clustering to cluster the informative genes based on their normalized binned expression profile to four clusters. Gene-gene correlation was calculated on the normalized binned expression profile of the informative genes (Z score normalization).

Gene modules clustering using NMF—Non-negative matrix factorization (NMF) was used – as an additional unsupervised clustering approach – to cluster the informative genes based on their normalized gene expression into four clusters. We computed the overlap between the gene modules found using *k-means* and NMF, using the hypergeometric test.

Gene modules score—To assign a gene module score to each cell, we calculated the mean normalized expression of the genes in each cluster to generate a mean module expression for each gene module. In each cell we reduced the lowest module expression

Author Manuscript Author Manuscript Author Manuscript Author Manuscript

value from all modules, normalized it to the sum expression of all the modules and assigned the highest scoring module as the dominant one of that cell. We ordered the cells based on their PC1 and PC2 coordinates. To assess the mid-infection transition, we computed the pairwise distance between cells along their PCA coordinates using the super module expression. The pairwise distance was calculated as a moving average using a running window (window size 10, step size 5), and binned into 5 groups according to their PCA coordinates.

***In-vivo* single cell data analysis—**Cell Ranger pipeline (V.3.0.0) was used for demultiplexing, mapping to the mouse genome (mm10) and counting umis for individual cells. Cells were filtered out if they had less than 1000 unique molecular identifiers (UMIs), and if more than 30% or 15% of their transcripts were ribosomal or mitochondrial genes, respectively. Expression was normalized to transcripts per median (TPM) and transformed using Freeman-Tukey transform (FTT). Cells from the infected sample were filtered by sequentially removing: 1. a cluster of cells inferred to be red blood cells according to their expression of hemoglobin genes, 2. a cluster of cells inferred to be lymphocytes according to their expression of marker genes such as Cd2, and 3. dying cells according to their expression of mitochondrial genes (Figure S6B). PCA was carried out on informative genes as in the analysis of the *ex vivo* experiments. Human and mouse orthologs were delineated using the Ensembl database (Howe et al., 2021). The mid-infection transition was assessed by computing the transcriptomic distance as unity minus the Pearson's correlation coefficient among the cells binned into 5 categories along the infection trajectory. Analyzing the PBS-infected cells (control, Figure S6C) we filtered a cluster of inferred lymphocytes and again computed a trajectory based upon the first two principal components. Gene, GO, and module expression profiles were smoothed using a moving average with a window size of twenty cells.

Supplementary Material

Refer to Web version on PubMed Central for supplementary material.

ACKNOWLEDGMENTS

We thank Adam Ratner, Igor Brodsky, Hervé Agaiss, Danielle A. Garsin, and Kamal Khanna for providing the bacterial strains in this study. We thank Adam Ratner, Jeff Weiser, and members of the Yanai lab for helpful advice and discussion. We thank Matt Maurano, Megan Hogan, Raven Luther, and the NYU Langone Genome Technology Center for sequencing. We thank Peter Smibert from the New York Genome Center for the generous gift of hashtag antibodies. This work was supported by grants R01AI143290 (I.Y.), R01AI137336 (B.S., V.J.T., and I.Y.), R01AI133977 (V.J.T.), and R01AI140754 (V.J.T. and B.S.). This work was also supported by the Lowenstein Foundation. F.K. was supported by 5T32AI100853–09, and K.A.L. was supported by a Cystic Fibrosis Postdoctoral Research Fellowship Award.

REFERENCES

Akira S, Uematsu S, and Takeuchi O (2006). Pathogen recognition and innate immunity. Cell 124, 783–801. [PubMed: 16497588]

Avital G, Avraham R, Fan A, Hashimshony T, Hung DT, and Yanai I (2017). scDual-Seq: mapping the gene regulatory program of Salmonella infection by host and pathogen single-cell RNA-sequencing. Genome Biol 18, 200. [PubMed: 29073931]

Author Manuscript Author Manuscript Author Manuscript Author Manuscript

Avraham R, Haseley N, Brown D, Penaranda C, Jijon HB, Trombetta JJ, Satija R, Shalek AK, Xavier RJ, Regev A, and Hung DT (2015). Pathogen cell-to-cell variability drives heterogeneity in host immune responses. Cell 162, 1309–1321. [PubMed: 26343579]

Bhattacharya M, Berends ETM, Chan R, Schwab E, Roy S, Sen CK, Torres VJ, and Wozniak DJ (2018). Biofilms release leukocidins to elicit extracellular trap formation and evade neutrophil-mediated killing. Proc. Natl. Acad. Sci. USA 115, 7416–7421. [PubMed: 29941565]

Björk L, Andersson J, Ceska M, and Andersson U (1992). Endotoxin and Staphylococcus aureus enterotoxin A induce different patterns of cytokines. Cytokine 4, 513–519. [PubMed: 1292633]

Blecher-Gonen R, Bost P, Hilligan KL, David E, Salame TM, Roussel E, Connor LM, Mayer JU, Bahar Halpern K, Tóth B, et al. (2019). Single-cell analysis of diverse pathogen responses defines a molecular roadmap for generating antigen-specific immunity. Cell Syst 8, 109–121.e6. [PubMed: 30772378]

Bossel Ben-Moshe N, Hen-Avivi S, Levitin N, Yehezkel D, Oosting M, Joosten LAB, Netea MG, and Avraham R (2019). Predicting bacterial infection outcomes using single cell RNA-sequencing analysis of human immune cells. Nat. Commun 10, 3266. [PubMed: 31332193]

Bumann D (2015). Heterogeneous host-pathogen encounters: act locally, think globally. Cell Host Microbe 17, 13–19. [PubMed: 25590757]

Cheng CS, Behar MS, Suryawanshi GW, Feldman KE, Spreafico R, and Hoffmann A (2017). Iterative modeling reveals evidence of sequential transcriptional control mechanisms. Cell Syst 4, 330–343.e5. [PubMed: 28237795]

Cheng Q, Behzadi F, Sen S, Ohta S, Spreafico R, Teles R, Modlin RL, and Hoffmann A (2019). Sequential conditioning-stimulation reveals distinct gene- and stimulus-specific effects of Type I and II IFN on human macrophage functions. Sci. Rep 9, 5288. [PubMed: 30918279]

Feezor RJ, Oberholzer C, Baker HV, Novick D, Rubinstein M, Moldawer LL, Pribble J, Souza S, Dinarello CA, Ertel W, and Oberholzer A (2003). Molecular characterization of the acute inflammatory response to infections with gram-negative versus gram-positive bacteria. Infect. Immun 71, 5803–5813. [PubMed: 14500502]

Flaherty RA, Borges EC, Sutton JA, Aronoff DM, Gaddy JA, Petroff MG, and Manning SD (2019). Genetically distinct Group B Streptococcus strains induce varying macrophage cytokine responses. PLoS One 14, e0222910. [PubMed: 31536604]

Flaherty RA, Aronoff DM, Gaddy JA, Petroff MG, and Manning SD (2021). Distinct group B sequence and capsule types differentially impact macrophage stress and inflammatory signaling responses. Infect. Immun 89, 006477–e720. 10.1128/IAI.00647-20.

Gomes T, Teichmann SA, and Talavera-López C (2019). Immunology driven by large-scale single-cell sequencing. Trends Immunol 40, 1011–1021. [PubMed: 31645299]

Gulati GS, Sikandar SS, Wesche DJ, Manjunath A, Bharadwaj A, Berger MJ, Ilagan F, Kuo AH, Hsieh RW, Cai S, et al. (2020). Single-cell transcriptional diversity is a hallmark of developmental potential. Science 367, 405–411. [PubMed: 31974247]

Hao S, and Baltimore D (2009). The stability of mRNA influences the temporal order of the induction of genes encoding inflammatory molecules. Nat. Immunol 10, 281–288. [PubMed: 19198593]

Hirayama D, Iida T, and Nakase H (2017). The phagocytic function of macrophage-enforcing innate immunity and tissue homeostasis. Int. J. Mol. Sci 19, E92. 10.3390/ijms19010092.

Holmgren AM, McConkey CA, and Shin S (2017). Outrunning the Red Queen: bystander activation as a means of outpacing innate immune subversion by intracellular pathogens. Cell. Mol. Immunol 14, 14–21. [PubMed: 27545071]

Howe KL, Achuthan P, Allen J, Allen J, Alvarez-Jarreta J, Amode MR, Armean IM, Azov AG, Bennett R, Bhai J, et al. (2021). Ensembl 2021. Nucleic Acids Res 49, D884–D891. [PubMed: 33137190]

Iwasaki A, and Medzhitov R (2015). Control of adaptive immunity by the innate immune system. Nat. Immunol 16, 343–353. [PubMed: 25789684]

Janeway CA Jr., and Medzhitov R (2002). Innate immune recognition. Annu. Rev. Immunol 20, 197–216. [PubMed: 11861602]

Author Manuscript Author Manuscript Author Manuscript Author Manuscript

Lacey KA, Gonzalez S, Yeung F, Putzel G, Podkowik M, Pironti A, Shopsin B, Cadwell K, and Torres VJ (2022). Microbiome-independent effects of antibiotics in a murine model of nosocomial infections. mBio 13.

Lange M, Bergen V, Klein M, Setty M, Reuter B, Bakhti M, Lickert H, Ansari M, Schniering J, Schiller HB, et al. (2022). CellRank for directed single-cell fate mapping. Nat. Methods 19, 159–170. [PubMed: 35027767]

Medzhitov R, and Janeway CA Jr. (1997). Innate immunity: impact on the adaptive immune response. Curr. Opin. Immunol 9, 4–9. [PubMed: 9039775]

Murray PJ, and Wynn TA (2011). Protective and pathogenic functions of macrophage subsets. Nat. Rev. Immunol 11, 723–737. [PubMed: 21997792]

Nau GJ, Richmond JFL, Schlesinger A, Jennings EG, Lander ES, and Young RA (2002). Human macrophage activation programs induced by bacterial pathogens. Proc. Natl. Acad. Sci. USA 99, 1503–1508. [PubMed: 11805289]

Parihar A, Eubank TD, and Doseff AI (2010). Monocytes and macrophages regulate immunity through dynamic networks of survival and cell death. J. Innate Immun 2, 204–215. [PubMed: 20375558]

Peters JM, Blainey PC, and Bryson BD (2020). Consensus transcriptional states describe human mononuclear phagocyte diversity in the lung across health and disease. Preprint at bioRxiv 10.1101/2020.08.06.240424.

Picelli S (2017). Single-cell RNA-sequencing: the future of genome biology is now. RNA Biol 14, 637–650. [PubMed: 27442339]

Qiu X, Hill A, Packer J, Lin D, Ma Y-A, and Trapnell C (2017a). Single-cell mRNA quantification and differential analysis with Census. Nat. Methods 14, 309–315. [PubMed: 28114287]

Qiu X, Mao Q, Tang Y, Wang L, Chawla R, Pliner HA, and Trapnell C (2017b). Reversed graph embedding resolves complex single-cell trajectories. Nat. Methods 14, 979–982. [PubMed: 28825705]

Ramond E, Jamet A, Coureuil M, and Charbit A (2019). Pivotal role of mitochondria in macrophage response to bacterial pathogens. Front. Immunol 10, 2461. [PubMed: 31708919]

Randis TM, Gelber SE, Hooven TA, Abellar RG, Akabas LH, Lewis EL, Walker LB, Byland LM, Nizet V, and Ratner AJ (2014). Group B Streptococcus b-hemolysin/cytolysin breaches maternal-fetal barriers to cause preterm birth and intrauterine fetal demise in vivo. J. Infect. Dis 210, 265–273. [PubMed: 24474814]

Ren K, and Torres R (2009). Role of interleukin-1beta during pain and inflammation. Brain Res. Rev 60, 57–64. [PubMed: 19166877]

Reyes-Robles T, Lubkin A, Alonzo F 3rd, Lacy DB, and Torres VJ (2016). Exploiting dominant-negative toxins to combat Staphylococcus aureus pathogenesis. EMBO Rep 17, 428–440. [PubMed: 26882549]

Rose HR, Holzman RS, Altman DR, Smyth DS, Wasserman GA, Kafer JM, Wible M, Mendes RE, Torres VJ, and Shopsin B (2015). Cytotoxic virulence predicts mortality in nosocomial pneumonia due to methicillin-resistant Staphylococcus aureus. J. Infect. Dis 211, 1862–1874. [PubMed: 25298028]

Rosenberg G, Yehezkel D, Hoffman D, Mattioli CC, Fremder M, Ben-Arosh H, Vainman L, Nissani N, Hen-Avivi S, Brenner S, et al. (2021). Host succinate is an activation signal for virulence during intracellular infection. Science 371, 400–405. [PubMed: 33479153]

Russo RC, Garcia CC, Teixeira MM, and Amaral FA (2014). The CXCL8/IL-8 chemokine family and its receptors in inflammatory diseases. Expert Rev. Clin. Immunol 10, 593–619.

Saliba A-E, Li L, Westermann AJ, Appenzeller S, Stapels DAC, Schulte LN, Helaine S, and Vogel J (2016). Single-cell RNA-seq ties macrophage polarization to growth rate of intracellular Salmonella. Nat. Microbiol 2, 16206. [PubMed: 27841856]

Sedger LM, and McDermott MF (2014). TNF and TNF-receptors: from mediators of cell death and inflammation to therapeutic giants - past, present and future. Cytokine Growth Factor Rev 25, 453–472. [PubMed: 25169849]

Shalek AK, Satija R, Shuga J, Trombetta JJ, Gennert D, Lu D, Chen P, Gertner RS, Gaublomme JT, Yosef N, et al. (2014). Single-cell RNA-seq reveals dynamic paracrine control of cellular variation. Nature 510, 363–369. [PubMed: 24919153]

Author Manuscript Author Manuscript Author Manuscript Author Manuscript

Sheu K, Luecke S, and Hoffmann A (2019). Stimulus-specificity in the responses of immune sentinel cells. Curr. Opin. Syst. Biol 18, 53–61. [PubMed: 32864512]

Shin S (2012). Innate immunity to intracellular pathogens: lessons learned from Legionella pneumophila. Adv. Appl. Microbiol 79, 43–71. [PubMed: 22569517]

Sica A, Erreni M, Allavena P, and Porta C (2015). Macrophage polarization in pathology. Cell. Mol. Life Sci 72, 4111–4126. [PubMed: 26210152]

Stoeckius M, Zheng S, Houck-Loomis B, Hao S, Yeung BZ, Mauck WM 3rd, Smibert P, and Satija R (2018). Cell Hashing with barcoded antibodies enables multiplexing and doublet detection for single cell genomics. Genome Biol 19, 224. [PubMed: 30567574]

Svensson V, Vento-Tormo R, and Teichmann SA (2018). Exponential scaling of single-cell RNA-seq in the past decade. Nat. Protoc 13, 599–604. [PubMed: 29494575]

Tong A-J, Liu X, Thomas BJ, Lissner MM, Baker MR, Senagolage MD, Allred AL, Barish GD, and Smale ST (2016). A stringent systems approach uncovers gene-specific mechanisms regulating inflammation. Cell 165, 165–179. [PubMed: 26924576]

Villani A-C, Satija R, Reynolds G, Sarkizova S, Shekhar K, Fletcher J, Griesbeck M, Butler A, Zheng S, Lazo S, et al. (2017). Single-cell RNA-seq reveals new types of human blood dendritic cells, monocytes, and progenitors. Science 356, eaah4573. 10.1126/science.aah4573. [PubMed: 28428369]

Viola A, Munari F, Sánchez-Rodríguez R, Scolaro T, and Castegna A (2019). The metabolic signature of macrophage responses. Front. Immunol 10, 1462. [PubMed: 31333642]

Wen M, Cai G, Ye J, Liu X, Ding H, and Zeng H (2020). Single-cell transcriptomics reveals the alteration of peripheral blood mononuclear cells driven by sepsis. Ann. Transl. Med 8, 125. [PubMed: 32175418]

Zhou J, Jin J-O, Du J, and Yu Q (2015). Innate immune signaling induces IL-7 production, early inflammatory responses, and sjögren's-like dacryoadenitis in C57BL/6 mice. Invest. Ophthalmol. Vis. Sci 56, 7831–7838. [PubMed: 26658504]

Author Manuscript Author Manuscript Author Manuscript Author Manuscript

Highlights

- The macrophage response to infection includes discrete cellular states
- The highly inflammatory state is composed of sequentially expressed gene modules
- Module dynamics depend on the stimulus, infection length, and presence of toxins

Author Manuscript Author Manuscript Author Manuscript Author Manuscript

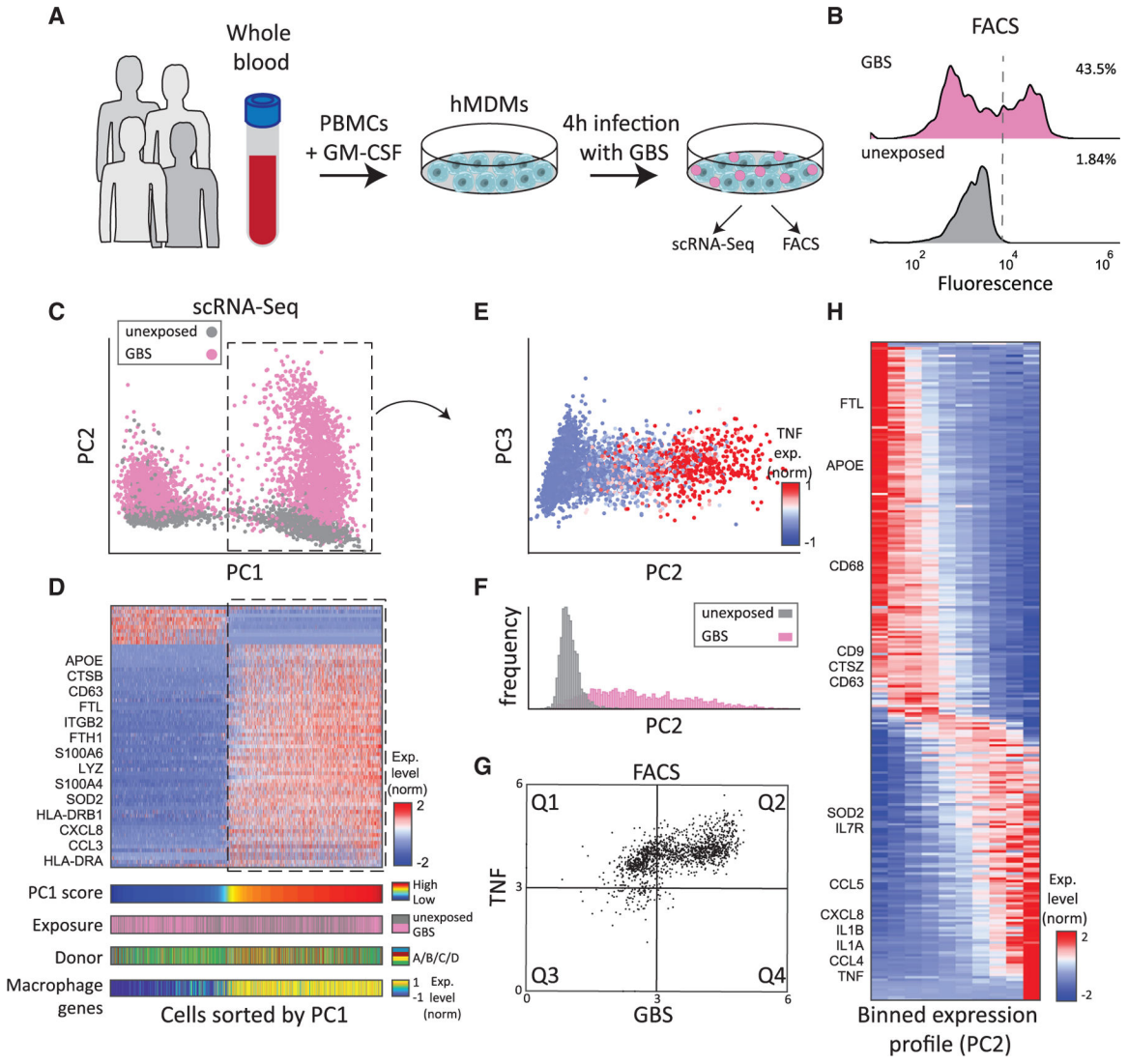

Figure 1. Immune response trajectory of macrophages during GBS infection

(A) Schematic of our approach. PBMCs from human blood were isolated, and monocytes were differentiated into macrophages (hMDM) using GM-CSF. hMDM were infected for 4 h with GBS, analyzed using flow cytometry and processed using scRNA-seq.

(B) Flow cytometry analysis of hMDM assessed the fraction of infected cells.

(C) PCA on single-cell transcriptomes reveals two groups. Colors indicate cells that were exposed to GBS (pink) and unexposed cells (gray). PCA was performed on 355 informative genes selected with mean threshold = 3 and fano threshold = 2 (see STAR Methods).

(D) Heatmap of expression of genes with high absolute PC1 loadings. Cells (columns) are sorted based on their PC1 score. The bars indicate PC1 score, GBS exposure, (exposed/unexposed, pink/gray, respectively), donor, and sum macrophage marker gene expression (low/high, cyan/yellow).

(E) Macrophage cells displayed by PC2 and PC3. Color indicates TNF expression levels.

(F) Histogram of the GBS-exposed cells (pink) and unexposed cells (gray) across PC2.

Author Manuscript Author Manuscript Author Manuscript Author Manuscript

(G) Flow cytometry analysis of GBS-exposed hMDMs measuring TNF levels and GBS fluorescence. Singlets were gated from all cells based on side scatter area by height. Unexposed and unstained cells were used to define GBS+ and TNF+ gates. Q1–4 consist of 444, 845, 9, and 75 cells respectively.

(H) Heatmap indicating gene expression across PC2. Binned expression profile of PC2 scores (see STAR Methods).

Author Manuscript Author Manuscript Author Manuscript Author Manuscript

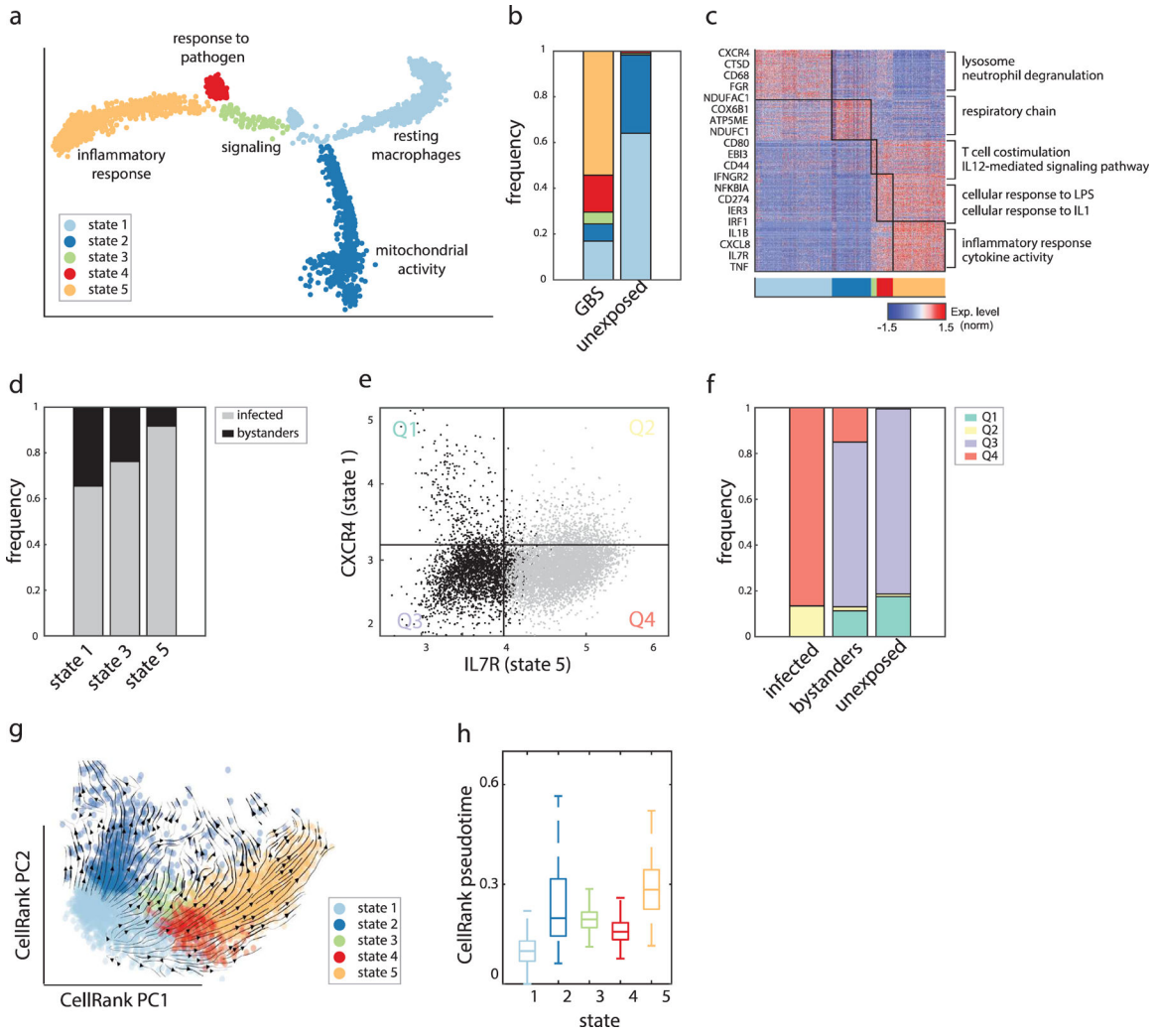

Figure 2. States of infection

(A) Trajectory analysis of GBS-exposed and unexposed macrophages using Monocle. Colors indicate transcriptional states. Monocle was performed on 458 informative genes selected with mean threshold = 2 and fano threshold = 2 (see STAR Methods).

(B) Bar plot indicating the distribution of the cells in each infection state for macrophages that were unexposed or exposed to GBS.

(C) Heatmap indicating the expression levels of the top 100 differentially expressed genes of each state compared with the other states. On the left are representative gene names, and on the right are representative Gene Ontology (GO) terms that are enriched for each state ($p < 0.05$). The bar below indicates the state.

(D) Bar plot representing the distribution of bystanders and unexposed cells in cells that are positive to the state staining. Cells were stained with fluorescently labeled CXCR4 antibody, CD80 antibody, and IL7R antibody as proxies for states 1, 3, and 5, respectively.

(E) Flow cytometry analysis of GBS-exposed hMDMs. Cells were stained with fluorescently labeled IL7R antibody and CXCR4 antibody, as proxies for states 5 and 1, respectively. Singlets were gated from all cells based on side scatter area by height. Unexposed and

Author Manuscript Author Manuscript Author Manuscript Author Manuscript

unstained cells were used to define IL7R+ and CXCR4+ gates. Color indicates infected (gray) or bystanders (black).
(F) Bar plot representing the distribution of the cells in each quadrant of the FACS plot for infected cells, bystanders, and unexposed cells. Color indicates the quadrant in (E).
(G) CellRank embeddings of macrophages colored by state. Arrows indicate the directionality of the cell-cell transition matrix computed by CellRank.
(H) Boxplot of CellRank pseudotime of macrophages by state.

Author Manuscript Author Manuscript Author Manuscript Author Manuscript

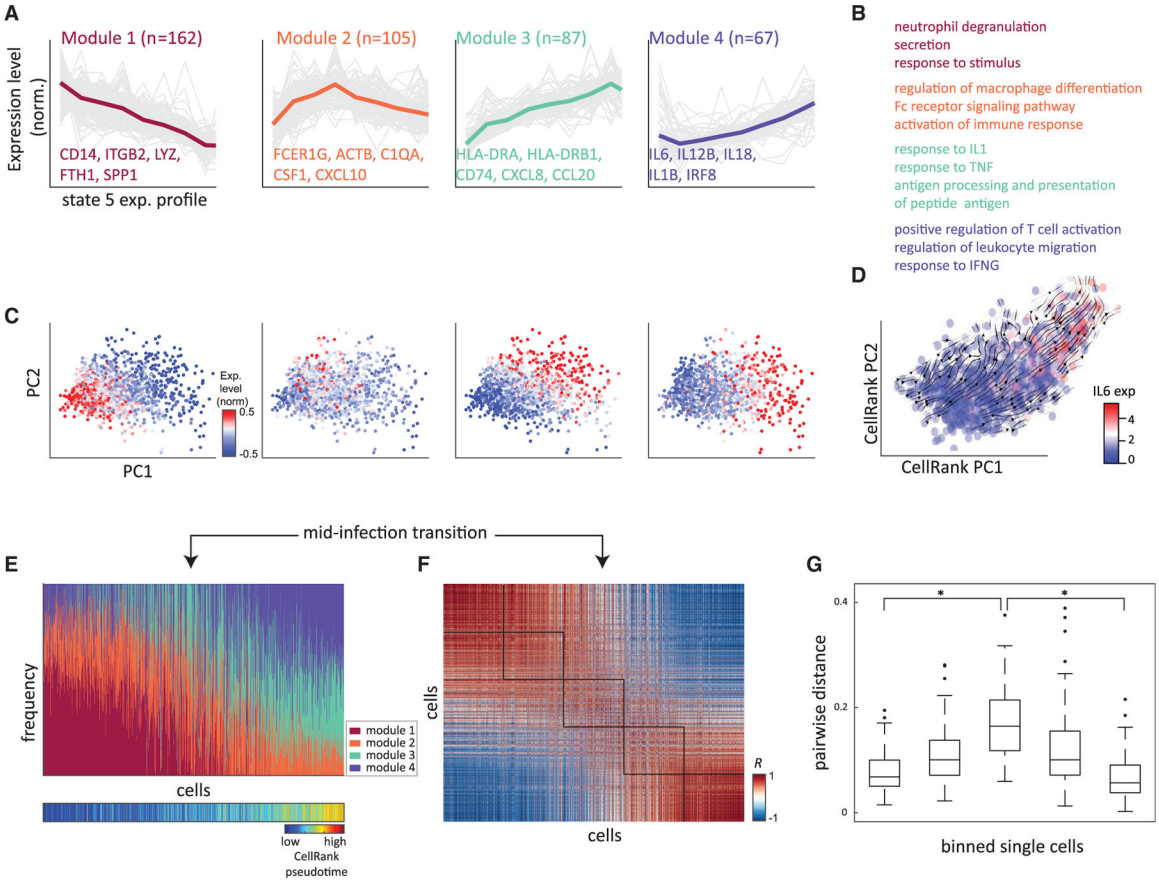

Figure 3. Gene expression modules of the inflammatory response

(A) Plots indicate the four gene modules (see STAR Methods); in gray are the expression profiles of the individual genes, and the mean expression of the module is indicated in color. Representative genes for each gene module are indicated below (see STAR Methods).

(B) A list of representative GO terms enriched in each gene module ($p < 0.05$). Color indicates the gene modules as in (A).

(C) PCA on single cells from state 5 colored by the mean expression of each gene module corresponding to the modules in (A). PCA was performed on 421 informative genes selected with mean threshold = 3 and fano threshold = 2 (see STAR Methods).

(D) CellRank embeddings of state 5 macrophages colored by normalized expression of IL6. Arrows indicate the directionality of the cell-cell transition matrix as computed by CellRank.

(E) Bar plots indicating the distribution of module expression levels in individual cells in state 5 (see STAR Methods). The colors indicate the gene modules as in (A) (top). CellRank pseudotime scores per cell (bottom). The cells are sorted by PC1 and PC2 coordinates.

(F) Heatmap representing the Pearson's correlation coefficient computed on the mean expression level of the gene modules in individual cells. The cells are sorted as in (E). Binned correlation used to calculate pairwise distance (in G) is indicated in black.

(G) Boxplots indicating the pairwise distance of the module scores between cells (*$p < 10^{-10}$).

Author Manuscript Author Manuscript Author Manuscript Author Manuscript

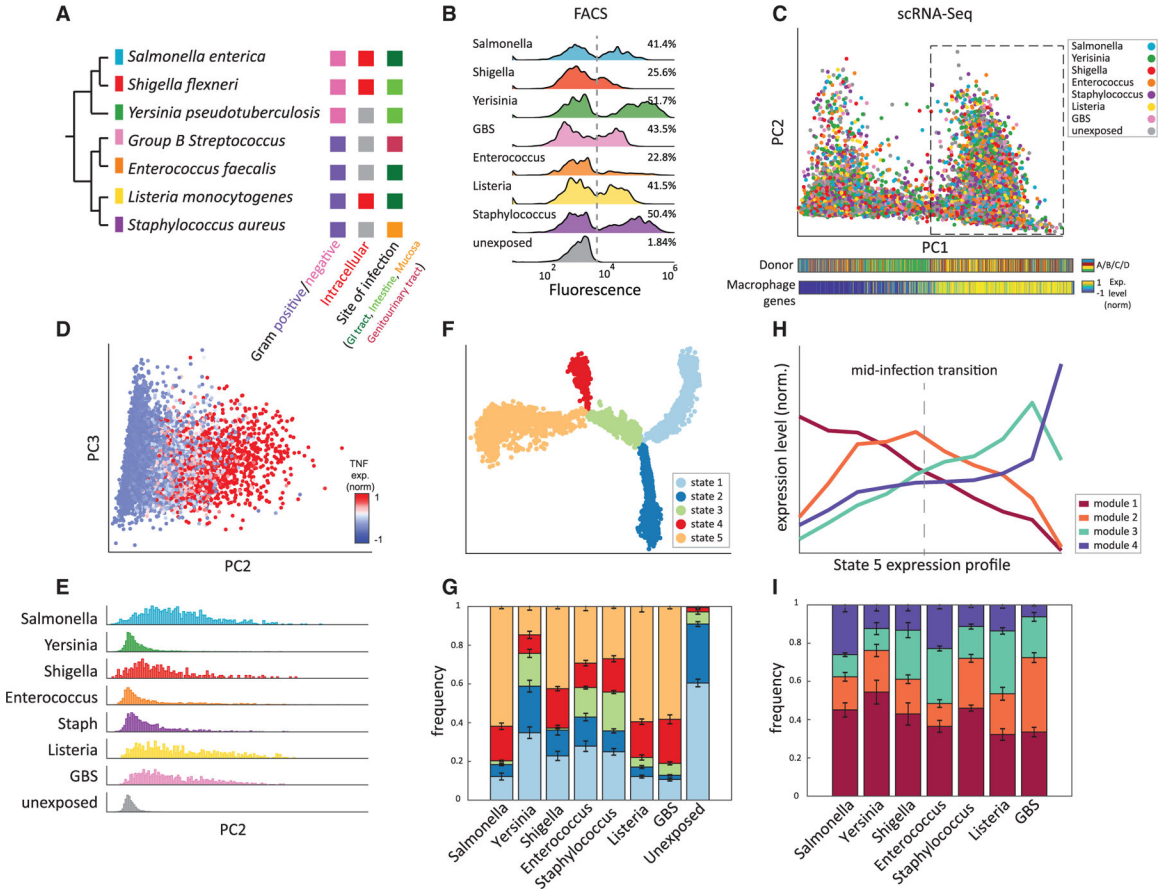

Figure 4. Conservation of infection states across diverse bacterial species

(A) Phylogenetic relationships between seven bacterial species. Gram staining, intracellular mode, and site of infection are indicated to the right.

(B) Flow cytometry analysis of hMDM assessed the fraction of infected cells (on the right). The colors indicate exposure to bacteria or unexposed (bacteria name on the left).

(C) PCA on hMDMs exposed to seven species for 4 h. Color indicates the bacterial exposure. Dashed box indicates the fully differentiated macrophage cluster. The bars below the plot indicate macrophage marker gene expression (see STAR Methods) and donor of origin of the PC1-sorted cells. PCA was performed on 320 informative genes selected with mean threshold = 2 and fano threshold = 2 (see STAR Methods).

(D) PC2 accounts for the trajectory of infection. Color indicates expression levels of TNF in the macrophages from (C).

(F) Histograms of the PC2 scores for macrophages exposed to each of the seven species or unexposed.

(G) Single-cell trajectory analysis using Monocle on macrophages exposed or unexposed to bacteria. Colors indicate states. Monocle was performed on 302 informative genes selected with mean threshold = 2 and fano threshold = 2 (see STAR Methods).

(H) Bar plots indicating the distribution of the cells in each infection state for hMDM that were exposed to different bacteria and unexposed cells. Error bars indicate the standard error among the four donor replicates.

Author Manuscript Author Manuscript Author Manuscript Author Manuscript

(I) Plot of gene module average expression profile across all infection conditions. Color indicates gene module as in Figure 3A.
(J) Bar plot indicating the distribution of the cells in each gene module of state 5 (see STAR Methods). Color indicates gene modules as in (G). Error bars are for standard error between the four donor replicates.

Author Manuscript Author Manuscript Author Manuscript Author Manuscript

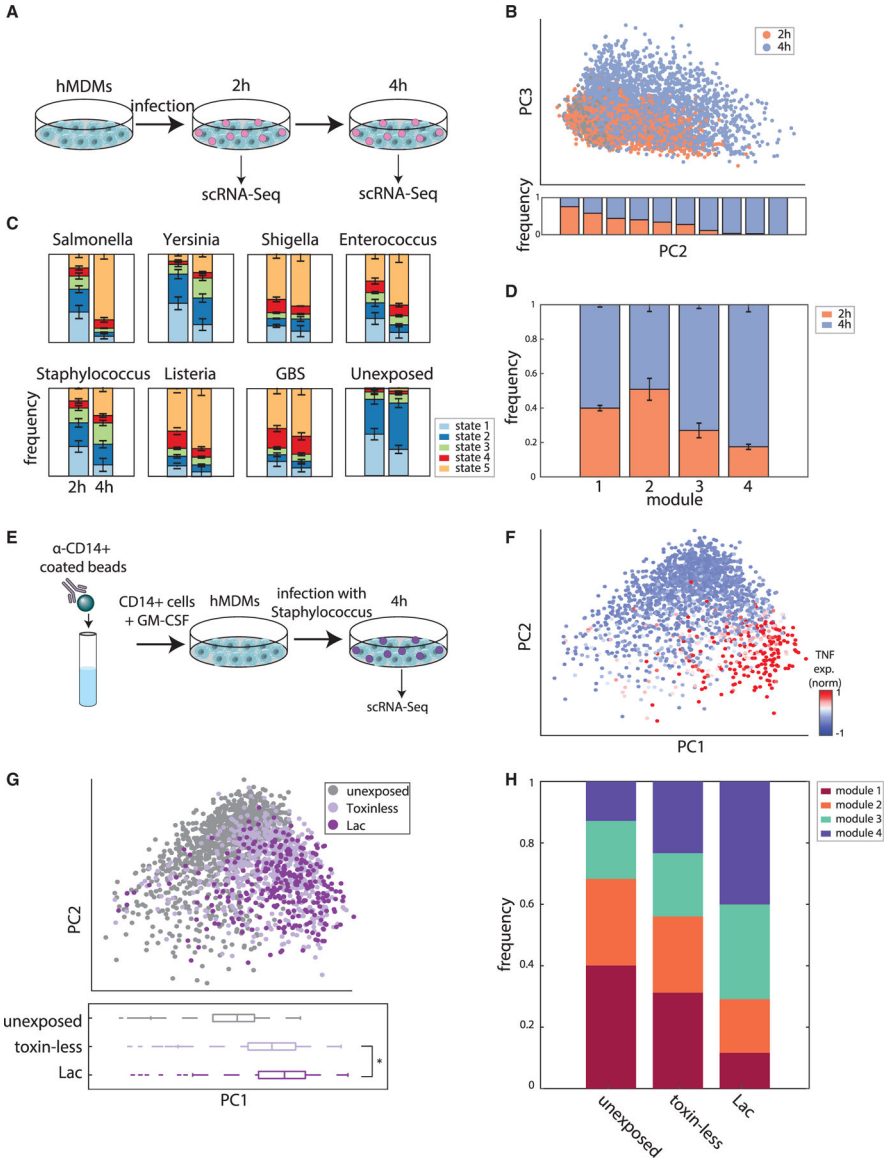

Figure 5. Dynamics of infection states across species

(A) hMDM were exposed and unexposed to bacteria for 2 and 4 h and processed using scRNA-seq.

(B) PCA on macrophages exposed and unexposed to seven species for 2 and 4 h. Color indicates unexposed cells and time of exposure to bacteria. PCA was performed on 325 informative genes selected with mean threshold = 2 and fano threshold = 2 (see STAR Methods). The bar below indicates the fraction of exposed cells from the 2- and 4-h infections across PC1 in (A).

(C) Barplots indicate the frequencies of the infection states after 2 h and 4 h of infection.

(D) Bar plot indicating the fraction of the cells from 2 to 4 h of infection in each gene module of state 5 (see STAR Methods). Color indicates 2 and 4 h of infection. Error bars indicate the standard error among the donor replicates.

Author Manuscript Author Manuscript Author Manuscript Author Manuscript

(E) Schematic of our approach. PBMCs from human blood were isolated, and CD14+ monocytes were selected and differentiated into macrophages (hMDM) using GM-CSF. hMDMs were then infected for 4 h with *Staphylococcus* and processed using scRNA-seq.
(F) PCA on macrophages colored by normalized expression of TNF. PCA was performed on 317 informative genes selected with mean threshold = 2, fano threshold = 2.
(G) PCA on macrophages colored by infection condition. Boxplots of PC1 scores between conditions (bottom, $*p < 10^{-3}$).
(H) Relative composition of state 5 modules within macrophages selected above a threshold of TNF expression.

Author Manuscript Author Manuscript Author Manuscript Author Manuscript

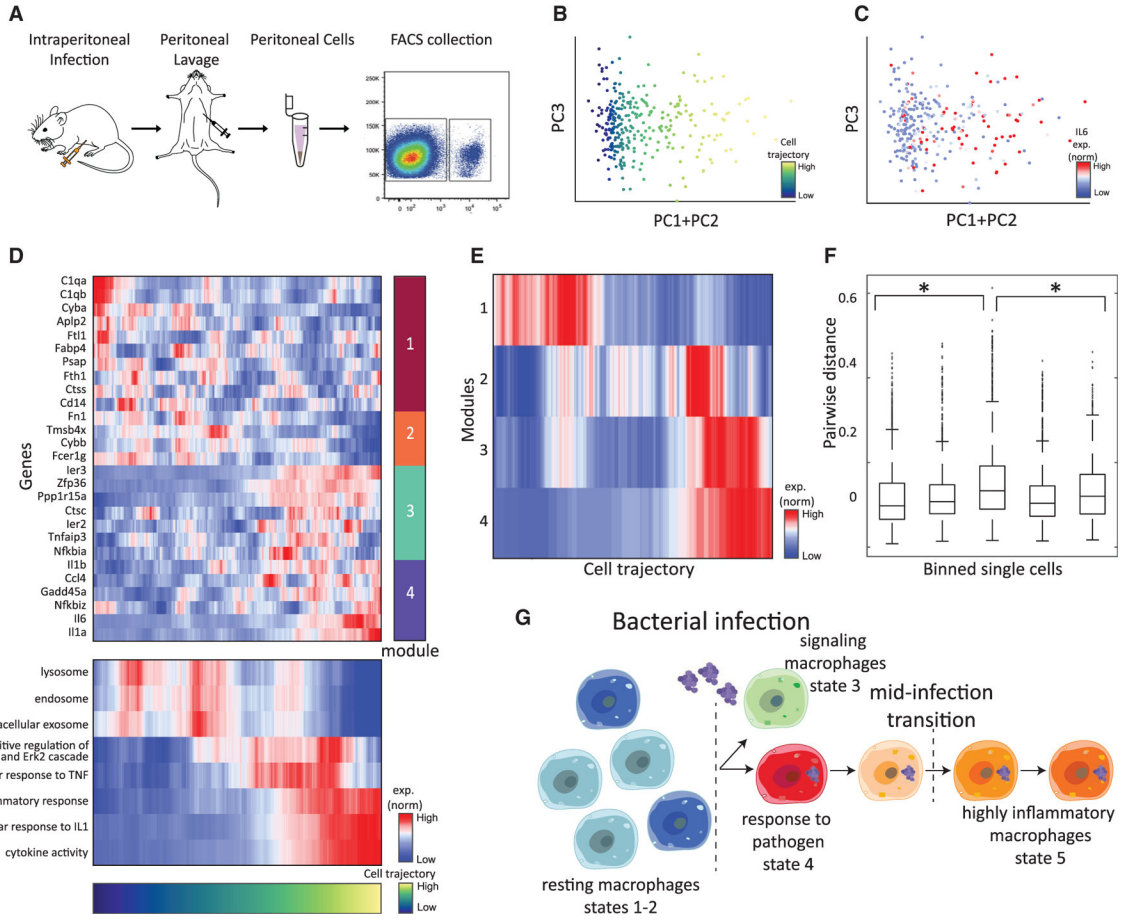

Figure 6. *In vivo* analysis of macrophage response modules in a model of peritoneal *Staphylococcus aureus* infection

(A) Mice were injected intraperitoneally with *S. aureus* or PBS. After 1 h, cells were collected by peritoneal lavage, and infected macrophages were sorted by FACS for downstream scRNA-seq analysis.

(B) PCA computed on 662 informative genes selected with mean threshold = 2 and fano threshold = 2 of infected macrophages colored according to Il6 expression.

(C) Cells are colored according to their trajectory score, which is calculated as the sum of PC1 + PC2 scores.

(D) Differentially expressed and upregulated genes selected from human modules expressed across the infection trajectory (top). Selected GO enrichment of human modules along the infection trajectory.

(E) Expression of human modules along the infection trajectory.

(F) Boxplots indicating the pairwise distance of the module scores between cells (*$p < 10^{-10}$).

(G) A model of the host response to bacterial infection. Colors indicate the states as in Figure 2A.

Author Manuscript Author Manuscript Author Manuscript Author Manuscript

KEY RESOURCES TABLE

REAGENT or RESOURCE	SOURCE	IDENTIFIER
Antibodies		
Human cell hashing antibody mix (HTO 1–10)	Peter Smibert	N/A
Pe/Cy7 TNF anti-human antibody	BioLegend	Cat# 502929; RRID: AB_2204080
Brilliant Violet CXCR4 anti-human antibody	BioLegend	Cat# 306517; RRID: AB_10901163
Pe/Cy7 CD80 antibody	BioLegend	Cat# 305217; RRID: AB_1877254
APC IL7R anti-human antibody	BioLegend	Cat# 351315; RRID: AB_10900814
Bacterial and virus strains		
Salmonella typhimurium SL1344	Igor Brodsky	N/A
Yersinia pseudotuberculosis IP32953	Igor Brodsky	N/A
Shigella flexneri 2a2457T	Hervé Agaisse	N/A
Enterococcus faecalis OG1RF	Danielle A. Garsin	N/A
Staphylococcus aureus USA300	Victor J. Torres	N/A
Listeria monocytogenes 10403S	Kamal Khanna	N/A
Streptococcus agalactiae (GBS) COH1	Adam Ratner	N/A
Staphylococcus aureus 4940	Victor J. Torres	N/A
Staphylococcus aureus 4875	Victor J. Torres	N/A
Staphylococcus aureus 4838	Victor J. Torres	N/A
Staphylococcus aureus 4884	Victor J. Torres	N/A
Staphylococcus aureus Th16	Victor J. Torres	N/A
Staphylococcus aureus LAC	Victor J. Torres	N/A
Staphylococcus aureus toxinless	Victor J. Torres	N/A
Staphylococcus aureus 9203	Victor J. Torres	N/A
Staphylococcus aureus 4906	Victor J. Torres	N/A
Biological samples		
Leukopacks	NYC Blood bank	N/A
Chemicals, peptides, and recombinant proteins		
PBS	Corning	21–040-CV
Ficoll	Sigma-Aldrich	17–1440-02
RPMI	Corning	10–040-CV
FBS	Fisher Scientific	16–000-044
HEPES	Fisher Scientific	BP299–100
ACK lysis buffer	Fisher Scientific	A1049201
PenStrep	Corning	30–002-Cl
GM-CSF	Sanofi	N/A
Penicillin	Millipore Sigma	5161–100MU
Streptomycin	VWR	0382–50G

Author Manuscript Author Manuscript Author Manuscript Author Manuscript

REAGENT or RESOURCE	SOURCE	IDENTIFIER
HSA	SeraCare	HS-420–1L
Human serum	Fisher Scientific	MP092930149
EDTA	Sigma-Aldrich	E6758–100G
LysE Lysis Buffer	BD Pharm	555899
Critical commercial assays		
EasySep™ Human CD14 Positive Selection Kit II	Stemcell Technologies	17858
10X Genomics Single Cell 3′ v3	10X Genomics	1000075
Deposited data		
Raw data	This work	GEO: GSE145862
Experimental models: Organisms/strains		
C57BL/6 mice	Jackson Laboratory	000664
Oligonucleotides		
PCR additive primer 5′GTGACTGGAGTTCAG ACGTGTGC*T*C (* Phosphorothioate bond)	IDT	N/A
Software and algorithms		
Cell Ranger pipeline (V.3.0.0)	10X Genomics	https://support.10xgenomics.com/single-cell-gene-expression/software/overview/welcome
CITE-seq-Count pipeline	Stoeckius et al., 2017	Github: https://github.com/Hoohm/CITE-seq-Count
Seurat package multi-modal data	Stoeckius et al., 2017	Github: https://github.com/satijalab/seurat/blob/master/vignettes/multimodal_vignette.Rmd
Monocle	Qiu et al. 2017a, 2017b	http://cole-trapnell-lab.github.io/monocle-release/
FlowJo software v10.6.1	Tree Star	https://www.flowjo.com/
CellRank v1.5.1	Lange et al. 2022	Github: https://github.com/theislab/cellrank
CytoTRACE kernel	Gulati et al. 2020; Lange et al. 2022	https://cytotrace.stanford.edu/
Code for this study	This work	Github; https://github.com/yanailab/Pathcourse https://doi.org/10.5281/zenodo.7011311